13

Investigation of the Effect of the Active Layer Composition of Organic Photosensitive Structures with a Bulk Heterojunction Based on Fullerene and Non-Fullerene Acceptors on Spectral Characteristics

© M.D. Pavlova, I.A. Lamkin, S.A. Tarasov

St. Petersburg State Electrotechnical University „LETI", St. Petersburg, Russia

e-mail: mdpavlova@etu.ru

Received October 24, 2025
Revised January 07, 2026
Accepted January 21, 2026

The spectral characteristics of organic photosensitive structures based on fullerene and non-fullerene acceptors were investigated. Structures based on the conjugated polymer PBDTT-DPP in combination with the fullerene acceptor PC71BM and the non-fullerene acceptor ITIC-F were fabricated, and their spectral and photoelectric characteristics were studied. It was shown that the structure based on the binary blend PBDTT-DPP:PC71BM exhibits limited sensitivity (11 mA/W at 796 nm) due to the small offset between the lowest unoccupied molecular orbital levels of the donor and acceptor. The replacement of the acceptor with the non-fullerene ITIC-F, which possesses a deeper lowest unoccupied molecular orbital level, allowed the spectral range to be extended to 1000 nm and the maximum photosensitivity to be increased to 100 mA/W (at 825 nm), however, a dip was observed in the spectrum at 800 nm. To eliminate this drawback, a photosensitive structure based on the PBDTT-DPP:PC71BM:ITIC-F blend was developed. It was established that the introduction of the fullerene acceptor into the binary blend based on PBDTT-DPP:ITIC-F eliminates the spectral dip in photosensitivity and facilitates stepwise charge carrier transfer. As a result, the developed structure exhibits a spectral response in the wavelength range of 400−950 nm, high photosensitivity of 130 mA/W (at 818 nm), and improved electrical characteristics. It has been demonstrated that the use of a combination of fullerene and non-fullerene acceptors in the active layer of the structure allows increasing the sensitivity of organic photosensitive structures.

Keywords: organic photosensitive structures, fullerene derivative, non-fullerene acceptor, spectral characteristics, spin-coating.

DOI: 10.61011/EOS.2026.02.63471.8677-25

Introduction

The current level of development of imaging technologies, optical communications, spectroscopy, biomedical diagnostics, and environmental monitoring is stimulating an active search for the new solutions in the field of designing photosensitive structures for the visible and near-infrared (IR) spectral ranges [1,2]. Traditionally, these areas employ devices based on inorganic semiconductors, which possess high charge carrier mobility and photochemical stability. However, these materials have a number of disadvantages, such as high production costs, complex technological processes, and low mechanical strength, limiting the possibility of creating flexible devices necessary for the development of „wearable" electronics devices [3].

An alternative is offered by photosensitive structures whose active layer is based on organic semiconductor materials. Their advantages include low cost of raw materials and synthesis processes, the possibility of using simple technologies to manufacture photosensitive structures based on them, including spin-coating and inkjet printing methods. Due to the low weight and high mechanical strength of organic compounds, photosensitive structures can be formed on flexible substrates [4]. Furthermore, an important advantage of organic semiconductors is the ability to finely tune the optical and electronic properties of the materials by modifying the molecular structure, which provides control over the position of energy levels and bandgap, absorption and photosensitivity spectra, as well as charge carrier mobility, opening up prospects for the development of compact, energy-efficient, and multifunctional devices [5]. Despite their advantages, the widespread adoption of organic photosensitive structures (OPSs) is prevented by the problems associated with the limited photochemical stability of some materials and low charge carrier mobility [6]. A key feature of OPS operation compared to devices based on inorganic semiconductors is the mechanism of generation and separation of charge carriers in organic semiconductors. Photon absorption causes generation of an exciton — a bound electron-hole pair, which must reach the interface of donor and acceptor materials (donor-acceptor interface) to dissociate into free carriers [7,8]. Since the exciton diffusion length, i.e., the distance an exciton can travel during its lifetime, is small (typically 5−15 nm) [9], the morphology of the active layer plays a crucial role in OPS efficiency. The active layer must simultaneously exhibit high absorption and enable efficient exciton dissociation, which imposes conflicting limitations. On the one hand, the active layer must be sufficiently

thick to ensure adequate absorption of incident radiation; on the other hand, its thickness should be comparable to the exciton diffusion length in the material; otherwise, exciton recombination will dominate over dissociation, leading to low photosensitivity of the fabricated devices [10].

The solution to this contradiction was the concept of the bulk heterojunction, in which the donor and acceptor are deposited simultaneously, forming an interpenetrating nanostructured network that creates numerous interfaces for efficient exciton dissociation, unlike planar structures where the donor and acceptor are sequentially deposited onto each other, resulting in a single lengthy interface [11]. However, in bulk heterojunction structures, there is a high probability of recombination of already separated charge carriers on their way to the electrodes, which limits the overall device efficiency. One method to limit charge carrier recombination is the creation of multicomponent active layers containing one donor and several acceptors (or vice versa) [12].

The introduction of a third component with thoroughly selected positions of the highest occupied and lowest unoccupied molecular orbital energy levels allows several tasks to be solved: expanding the absorption spectral range, creating a stepwise energy diagram to facilitate charge separation and reduce recombination losses, and optimizing the layer morphology to improve charge carrier transport [13]. In particular, the use of a narrow-bandgap acceptor in combination with a wider-bandgap material allows expanding the spectral sensitivity range.

Despite the significant progress in the field of organic photosensitive structures, their sensitivity in the near-IR spectral range remains limited due to the features of photogeneration and charge carrier transfer in organic semiconductors. Typically, the spectral sensitivity range of such structures is limited to wavelengths up to 800 nm, and in the case of a wider operating spectral range, the near-infrared range experiences a decrease in spectral sensitivity [14,15]. In this regard, the development of active layers that expand the spectral range of photosensitivity while maintaining high electrical characteristics of the devices is a relevant task. Extending the spectral response into the long-wavelength region is usually achieved by using narrow-bandgap donors based on conjugated donor-acceptor polymers and non-fullerene acceptors, which can significantly enhance absorption in the long-wavelength region of the spectrum; however, in practice, this is often accompanied by deterioration of the active layer morphology and higher probability of recombination losses. At the same time, fullerene acceptors, possessing more favorable electron-transport properties, provide efficient electron transfer and suppress recombination, but do not sufficiently extend the spectral response into the near-infrared region [16]. This necessitates the search for compromise solutions combining the advantages of both types of acceptors within a single active layer.

The aim of this paper is to develop and investigate the influence of the composition of organic photosensitive structures with a bulk heterojunction based on an active layer containing fullerene and non-fullerene acceptors on the spectral characteristics and electrical parameters, as well as methods to extend the spectral range and to increase photosensitivity in the near-IR spectral range.

1. Materials and methods

1.1. Donor, acceptors

Poly {2,6′-4,8-di(5-ethylhexylthienyl)benzo[1,2-b;3,4-b]dithiophene-alt-5,5′-dibutyloctyl-3,6-bis(5-thiophene-2-yl)pyrrolo[3,4-c]pyrrole-1,4-dione} (PBDTT-DPP), the structure of which is shown in Fig. 1, *a* was chosen as the donor. This is a narrow-bandgap conjugated polymer consisting of donor-acceptor units, where benzodithiophene acts as the donor and diketopyrrolopyrrole as the acceptor [17]. The positions of the highest occupied molecular orbital (HOMO) and lowest unoccupied molecular orbital (LUMO) energy levels are -5.3 eV and -3.63 eV, respectively, the bandgap (E_g) is 1.67 eV.

The fullerene derivative [6,6]-phenyl C71 butyric acid methyl ester (PC71BM) was used as an acceptor; it is one of the most widely used electron-conducting materials for creating organic optoelectronic devices [18]. The molecular structure of PC71BM is shown in Fig. 1, *b*. Energies of HOMO- and LUMO-levels are -6.0 eV and -3.9 eV respectively, E_g is 2.1 eV.

To improve the absorption in the long-wavelength area of the spectrum, a narrow-bandgap non-fullerene acceptor was used — 3,9-bis(2-methylene-((3-(1,1-dicyanomethylene)-6,7- difluoro)-indanone))-5,5,11,11-tetrakis(4-hexylphenyl)-dithieno[2,3-d:2′,3′-d′]-s- indaceno[1,2-b:5,6-b′]dithiophene (ITIC-F), the molecular structure of which is shown in Fig. 1, *c*. The position of the energy levels complies with -5.7 eV for HOMO and -4.1 eV for LUMO, and the energy gap is 1.6 eV.

1.2. Samples creation

The studied samples were manufactured, and their parameters were measured under normal room conditions in air, without the use of an inert atmosphere. Within each experiment, a batch of 10 samples was created.

The spin-coating method was used to form the photosensitive structures. Glass coated with a thin layer of FTO, serving as a transparent anode, was used as substrates. The substrates were cleaned in an ultrasonic bath for 20 min, then washed in isopropyl alcohol and annealed for 10 min at 180 °C to remove organic contaminants and adsorbed moisture. Simultaneously, a solution to form the active layer by spin-coating was prepared. The donor and acceptor materials were dissolved in a common volume of solvent (chlorobenzene); the solution concentration was 5 mg/ml, while the donor-to-acceptor ratio was varied to select the active layer composition providing for the highest sensitivity of the samples. The spin-coating time for all samples was 30 s, the volume of deposited solution was 60 μl, and

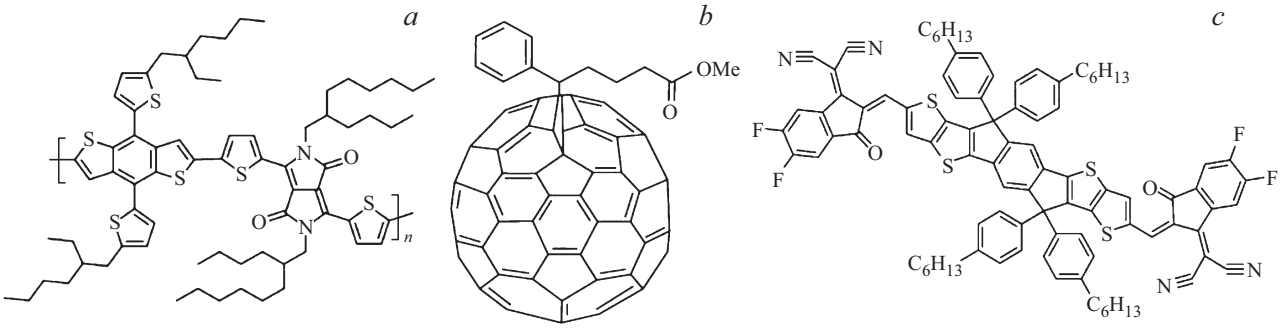

Figure 1. Molecular structures of PBDTT-DPP (*a*), PC71BM (*b*) and ITIC-F (*c*).

the substrate rotation speed during active layer formation was 1000 rpm, as this speed produces the most uniform films in terms of thickness. After depositing the active layer onto the substrate, annealing was performed at 70 °C for 7 min to remove residual solvent and form the structure. Then, a cathode based on an eutectic alloy of indium, gallium, and tin (InGaSn) was formed on top of the active layer using a mask with circular holes of 5 mm diameter. Fig. 2 shows schematic images of the created structures.

1.3. Absorption spectra

When measuring the absorption spectra, 25 points were studied on each sample, chosen so that the entire area of the sample, including edge points, was investigated.

The absorption spectra of the films were measured using a USB4000 fiber-optic spectrometer (Ocean Optics). The radiation source was an MR11 halogen lamp. To eliminate the influence of external illumination, a light-tight box housing the radiation source and sample holder was used. The spectra were measured before cathode formation.

1.4. Photosensitivity spectra

Photosensitivity spectra were measured in 5 points located in the central region of the samples and chosen to minimize edge effects and exclude electrical interaction between neighboring contacts.

Photosensitivity spectra were measured using an automated laboratory setup consisting of an incandescent lamp, a collimator system, a monochromator with an M266 diffraction grating (Solar), an SR830 lock-in amplifier (Stanford Research Systems), and a PC. The laboratory setup was controlled by a PC via specialized software developed in LabView, which also provided data recording and imaging. All measurements were carried out under short-circuit conditions. The environmental parameters and the power of the incident optical radiation remained unchanged. The setup was calibrated for sensitivity using a reference silicon photodetector.

Analysis of the distribution of the measured spectral dependencies showed that the standard deviation of absorption over the sample area did not exceed 8 %, while for photosensitivity spectra the corresponding deviation was no more than 5 %, indicating acceptable uniformity and reproducibility of the studied samples. Analysis of the deviation distribution showed their comparable nature across the entire studied spectral range, without a pronounced dependence on wavelength; therefore, the averaged spectral dependences are presented in this paper.

1.5. Electrical parameters

Short-circuit current density and open-circuit voltage were determined by measuring light current-voltage curves (CVC). The dark current was calculated from the reverse branch of the CVC measured without illumination. CVC measurements were carried out using a Keithley 2401 sourcemeter. An incandescent lamp calibrated against a silicon reference solar cell was used as the radiation source.

2. Analysis of the results

At the first stage of the study, structures with an active layer based on a blend of PBDTT-DPP and PC71BM were created. A schematic image of the studied structure of FTO/PBDTT-DPP:PC71BM/InGaSn type is shown in Fig. 2, *a*. The bandgaps of PBDTT-DPP and PC71BM are 1.67 eV and 2.1 eV, respectively. It follows that the greatest absorption of PBDTT-DPP and PC71BM occurs in the visible spectral range. To study the absorption spectra, a series of samples based on individual materials and the PBDTT-DPP:PC71BM blend (with a donor-to-acceptor ratio of 1:1) were created; the measurement results are shown in Fig. 3. The absorption of PBDTT-DPP-based films covers the wavelength range from 400 to 860 nm with maxima at wavelengths of 690 and 760 nm, due to intramolecular charge transfer [14]; the full width at half maximum (FWHM) is 170 nm. The absorption of PC71BM does not have a pronounced peak in the visible range; the main absorption of optical radiation occurs at wavelengths of 400–800 nm. The absorption of the blend-based film is the sum of the absorption curves of the pure materials; the highest absorption occurs in the wavelength range of 400–870 nm with maxima at 667 and 756 nm; the FWHM

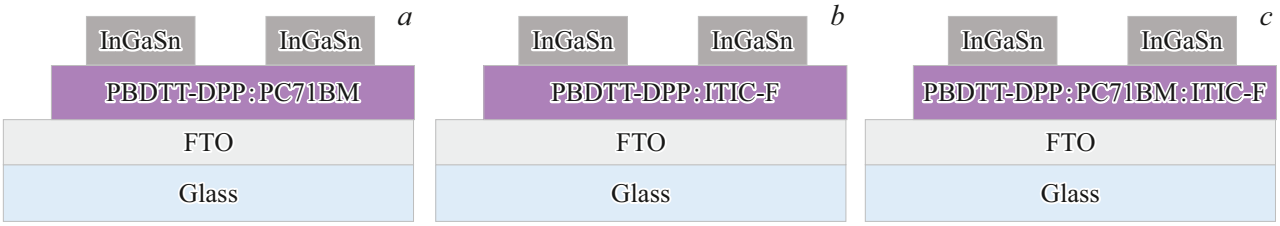

Figure 2. Schematic images of studied structures.

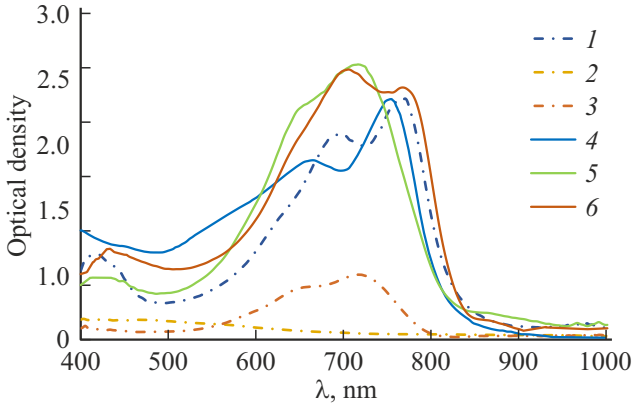

Figure 3. Absorption spectra of films based on: PBDTT-DPP — *1*, PC71BM — *2*, ITIC-F — *3*, PBDTT-DPP:PC71BM — *4*, PBDTT-DPP:ITIC-F — *5*, PBDTT-DPP:PC71BM:ITIC-F — *6*.

is 220 nm. Thus, the material blend exhibits high absorption in the visible spectral range, with a predominance in the red and near-infrared ranges.

During the fabrication of OPSs, the influence of the donor-to-acceptor ratio in the active layer composition on the photosensitivity intensity was studied; samples with donor-to-acceptor ratios of (1:1), (2:1), (1:2), (4:1), and (1:4) were created. Fig. 4, *a* shows the energy diagram of the studied structure. The measurement results of the spectral dependences of photosensitivity are shown in Fig 4, *b*.

For the samples with a higher donor concentration, i. e., ratios (2:1) and (4:1), the structures exhibit weak photosensitivity, and noise dominates the spectral dependence, which can be explained by the formation of an insufficient number of donor-acceptor interfaces necessary for efficient exciton dissociation. At a ratio of (1:1), photosensitivity increases, and the signal becomes distinguishable; the spectrum covers the wavelength range from 400 to 900 nm, and the highest signal is observed in the range of 760 to 830 nm. The maximum photosensitivity was 2 mA/W at a wavelength of 800 nm. Increasing the proportion of the acceptor component, conversely, promotes an increase in donor-acceptor interfaces and the formation of electron transport channels. For the samples with a donor-to-acceptor ratio of (1:2), an increase in photosensitivity intensity of almost 5 times is observed. The maximum photosensitivity corresponds to a wavelength of 796 nm and

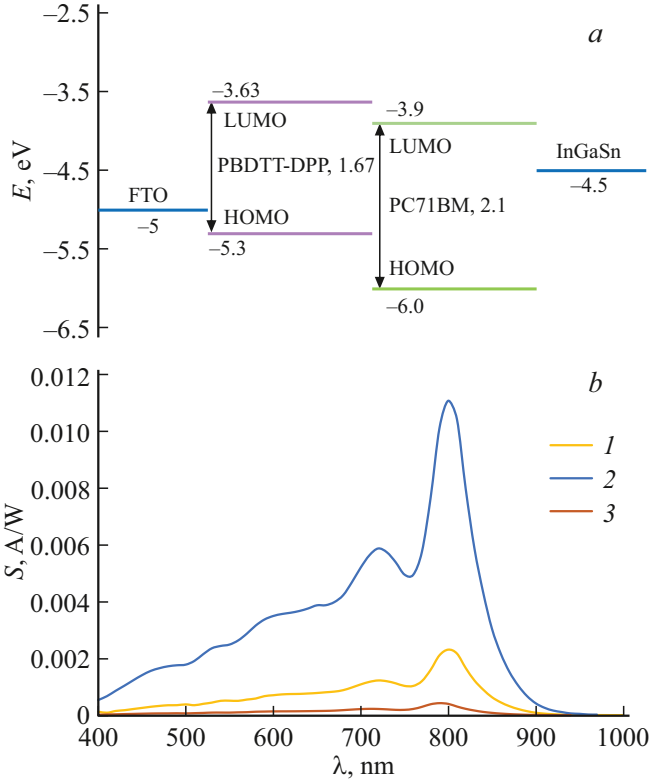

Figure 4. (*a*) Energy diagram of FTO/PBDTT-DPP:PC71BM/InGaSn structure. (*b*) Photosensitivity spectra of structures with different concentration of donor and acceptor: (1:1) — *1*, (1:2) — *2*, (1:4) — *3*.

amounts to 11 mA/W, which is determined by transitions in PBDTT-DPP. With a further increase in the acceptor proportion, the photosensitivity level decreases, which can be explained by the deterioration of film morphology due to PC71BM aggregation, resulting in a maximum photosensitivity intensity of only 0.4 mA/W. Thus, the optimal active layer composition is a donor-to-acceptor ratio of (1:2). For the studied samples, the short-circuit current density was 0.16 mA/cm^2, and the open-circuit voltage was 0.5 V. The dark current density was 100 nA/cm^2.

The photocurrents and sensitivity of the studied samples turned out to be low, which may be caused by the small difference in the LUMO energies of the donor and acceptor,

and consequently, a low built-in field necessary for exciton movement to the hetero-interface [19].

To increase the built-in field and for greater localization of photosensitivity in the near-IR spectral range, at the second stage of the study, the acceptor was replaced with ITIC-F, which has a deeper LUMO level (−4.1 eV) and a smaller bandgap of 1.6 eV compared to PC71BM. Fig. 2, *b* shows a schematic image of the structure under consideration.

To study the absorption spectra, samples based on individual materials and the PBDTT-DPP:ITIC-F blend (with a donor-to-acceptor ratio of 1:1) were created. The measurement results are shown in Fig. 3. ITIC-F exhibits the highest absorption in the wavelength range from 550 to 800 nm with maxima at wavelengths of 654 and 722 nm, and the FWHM is 175 nm. The absorption spectrum of films based on the PBDTT-DPP:ITIC-F blend has more intense absorption in the wavelength range from 622 to 745 nm compared to samples based on PBDTT-DPP:PC71BM, which is due to the contribution of ITIC-F. The maximum absorption of films based on the PBDTT-DPP:ITIC-F blend occurs at 716 nm; the FWHM was 177 nm.

A study was conducted on the influence of donor and acceptor concentration in the active layer based on the PBDTT-DPP:ITIC-F blend on the spectral dependence of photosensitivity. As previously established, increasing the proportion of the donor component does not have a significant positive effect on increasing the OPS photoresponse due to the deterioration of active layer morphology and the formation of isolated donor domains, which reduces the number of active donor-acceptor interfaces. Therefore, only the effect of increasing the acceptor component of the active layer was evaluated. The results are shown in Fig. 5, *b*. Fig. 5, *a* shows the energy diagram of the studied structures.

For the studied samples, the photosensitivity spectrum covers the wavelength range from 450 to 1000 nm and has two pronounced maxima. For the structure with equal donor and acceptor content, the first maximum is observed at a wavelength of 740 nm, the second — at 830 nm. For the structure with a higher ITIC-F content, the maxima are slightly shifted to the blue region and correspond to wavelengths of 736 and 825 nm. The spectrum also exhibits a short-wavelength shoulder, which may be caused by transitions from deeper molecular orbitals of the donor. At the same time, for the structure with an excess of acceptor, the photosensitivity in the wavelength range from 800 to 1000 nm is significantly reduced, which is explained by a decrease in the contribution of donor component absorption. Therefore, to develop OPSs with high photoresponse in the near-infrared spectral range, it is preferable to use equal concentrations of PBDTT-DPP and ITIC-F. For the structure with a donor-to-acceptor ratio of (1:1), the maximum photosensitivity was 100 mA/W (at 825 nm), short-circuit current density was 1.1 mA/cm^2, open-circuit voltage was 0.75 V, and dark current density was 130 nA/cm^2.

The photosensitivity spectra of the structures based on PBDTT-DPP exhibit a pronounced dip at wavelengths of

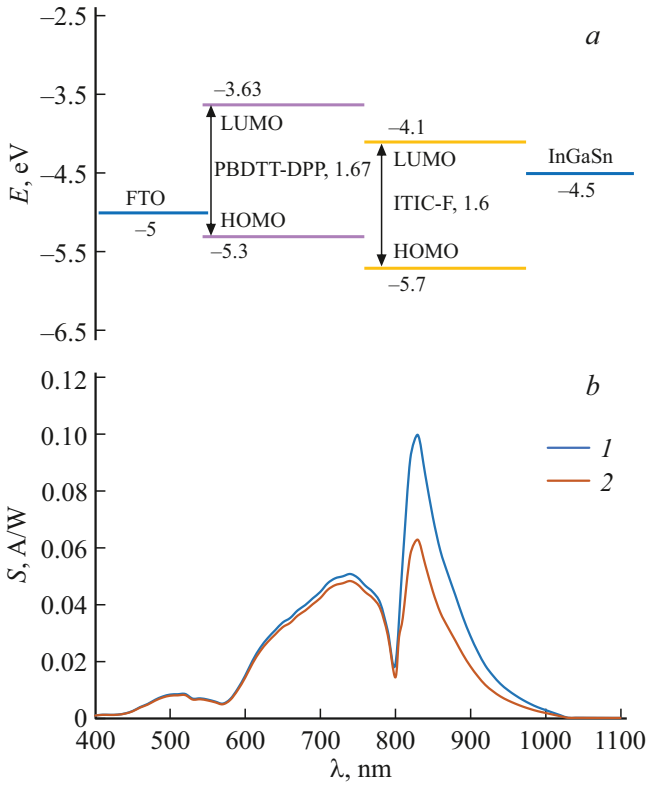

Figure 5. (*a*) Energy diagram of FTO/PBDTT-DPP:ITIC-F/InGaSn structure. (*b*) Photosensitivity spectra of structures with different concentration of donor and acceptor: (1:1) — *1*, (1:2) — *2*.

750 nm for samples based on the PBDTT-DPP:PC71BM blend and 800 nm for samples based on the PBDTT-DPP:ITIC-F blend, despite the retention of noticeable optical absorption. The optical bandgap of the PBDTT-DPP polymer is ∼ 1.52 eV. Excitation near this energy likely predominantly leads to the formation of intramolecular charge transfer states localized on diketopyrrolopyrrole (DPP), which are characterized by a high Coulomb binding energy of the electron-hole pair and limited spatial delocalization. Due to the weak binding of such states with transport levels and intermolecular charge transfer channels, their dissociation probability is reduced, which manifests as a dip in photosensitivity.

However, with a further increase in excitation wavelength, the excitation begins to affect lower-energy states associated with the donor-acceptor interface formed between the HOMO of PBDTT-DPP and the LUMO of the acceptor. Such states possess lower binding energy, which increases their dissociation probability in the presence of the device's built-in electric field.

The shift in the dip position when using different acceptors is associated with a change in the energy alignment of the LUMO levels and the energy of the intermolecular charge transfer state at the PBDTT-DPP/acceptor interface. For acceptors with a deeper LUMO level, ITIC-F, the energy gap between the LUMO of DPP fragments and

the LUMO of the acceptor decreases, which stabilizes the intermolecular charge transfer states and shifts their energy position towards lower energies (longer wavelengths). As a result, the spectral region where competition occurs between the localized intramolecular transfer states and the efficiently dissociating intermolecular charge transfer state shifts, changing the position of the photosensitivity minimum. Thus, the dip reflects the spectral transition between intramolecular and intermolecular charge transfer modes, and its position is determined by the combined contribution of the electronic structure of PBDTT-DPP and the energy of the acceptor used.

To suppress the dip in the photosensitivity spectrum of the PBDTT-DPP:ITIC-F-based structures, PC71BM was added to the active layer composition. The introduction of the fullerene acceptor should promote the formation of the additional electron transfer pathways and reduce the probability of charge carrier recombination, which will restore photosensitivity in this spectral region. The concentration of the donor and acceptors equal to (1:0.5:0.5) was used for sample fabrication. The materials were dissolved in a common volume of solvent. The structure of experimental samples based on the PBDTT-DPP:PC71BM:ITIC-F blend is shown in Fig. 2, *c*.

The absorption spectrum of the film based on the three-component blend lies in the wavelength range from 400 to 900 nm with a predominance in the red region, as shown in Fig. 3. The absorption maximum is observed at a wavelength of 709 nm, determined by absorption in the PBDTT-DPP:ITIC-F blend; a lower intensity maximum at 762 nm wavelength arises from absorption in the PBDTT-DPP:PC71BM blend, which also contributes slightly to absorption in the short-wavelength region of the spectrum (from 400 to 565 nm).

Fig. 6, *a* shows the energy diagram of the studied FTO/PBDTT-DPP:PC71BM:ITIC-F/InGaSn structures; Fig. 6, *b* shows the photosensitivity spectrum. For clarity, the photosensitivity spectra of the structure based on the PBDTT-DPP:ITIC-F and PBDTT-DPP:PC71BM blends are also shown.

The photosensitivity spectrum of the PBDTT-DPP:PC71BM:ITIC-F-based samples lies in the wavelength range from 400 to 950 nm. The maximum photosensitivity corresponds to a wavelength of 818 nm and amounts to 130 mA/W, which is 30 mA/W higher than for the structure without the fullerene derivative. Additionally, the dip at a wavelength of 800 nm was successfully eliminated from the photosensitivity spectrum. This result agrees with data from other authors [14,15,20–22]; however, these studies use more complex device configurations, including transport layers, or sample fabrication technologies requiring an inert gas atmosphere. The electrical parameters of the studied structure were also improved. The short-circuit current density of the sample was 2.2 mA/cm^2, which is 2 times higher than that of the structure without the addition of PC71BM, with an open-circuit voltage of 0.8 V. The dark

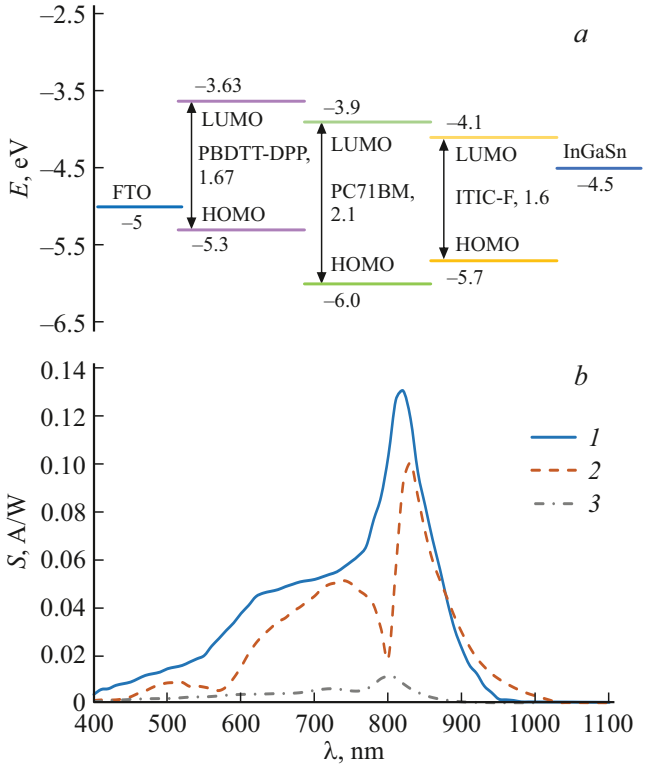

Figure 6. (*a*) Energy diagram of FTO/PBDTT-DPP:PC71BM:ITIC-F/InGaSn structure. (*b*) Photosensitivity spectra of structures based on blends: PBDTT-DPP:PC71BM:ITIC-F — *1*, PBDTT-DPP:ITIC-F — *2*, PBDTT-DPP:PC71BM — *3*.

current density was 68 nA/cm^2, which is almost 2 times lower than for the samples without the fullerene derivative.

Thus, the combination of fullerene and non-fullerene acceptors allowed extending the spectral range of photosensitivity compared to the structure containing only PC71BM, as well as increasing the signal intensity compared to samples based on two-component blends, which can be explained using Fig. 7 showing the most probable charge carrier transfer pathways in the studied OPS.

Pathways „*A*“ and „*B*“ are similar to the processes in the binary blends PBDTT-DPP:PC71BM and PBDTT-DPP:ITIC-F, respectively. Pathway „*B*“ is preferable since the useful signal with this charge carrier transfer pathway is higher. Pathways „*C*“ and „*D*“ only occur in the three-component blend, with pathway „*C*“ being more energetically favorable, contributing to the improvement of the parameters of the studied structure. In this case, stepwise electron transfer from PBDTT-DPP to ITIC-F via PC71BM is possible, which facilitates charge carrier separation and reduces their recombination, contributing to better current transport in the structure. Simultaneously, due to the deep HOMO level of PC71BM, a potential barrier is formed for holes localized in the donor, which also helps reduce the probability of recombination at the donor-acceptor interface. Pathway „*D*“, conversely, is unfavorable due to the formation of a potential barrier for electrons by

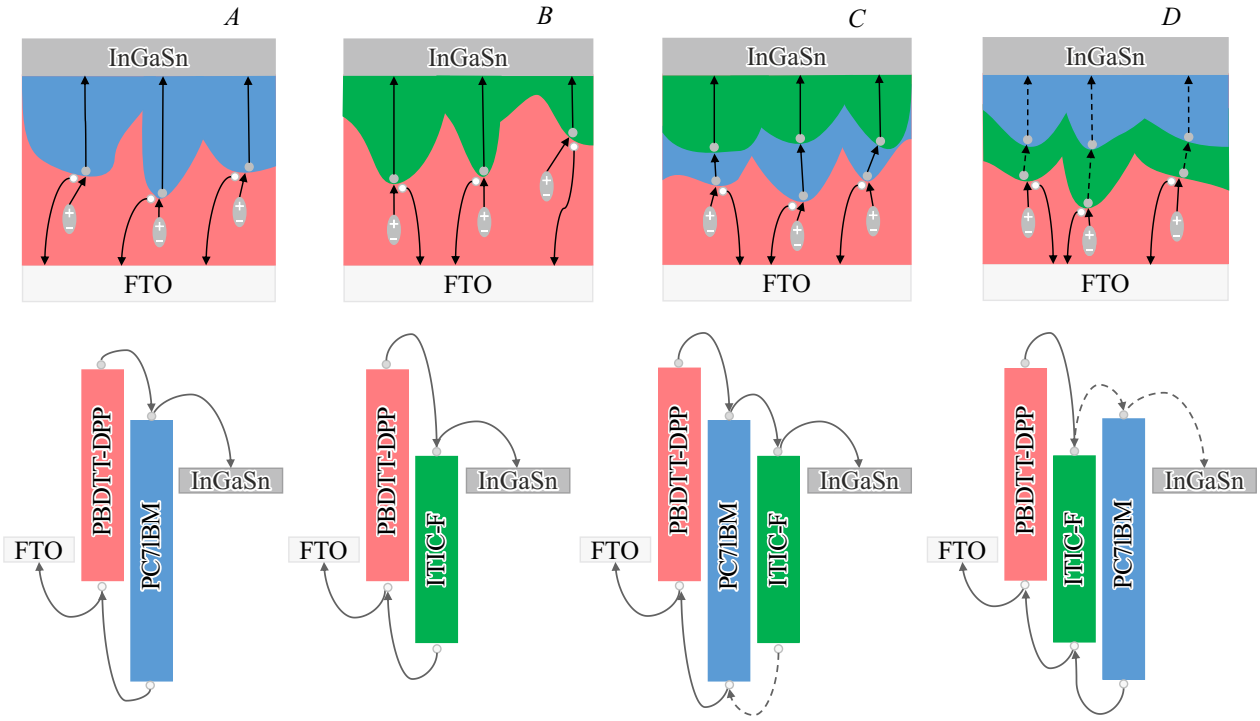

Figure 7. Most probable pathways for charge carrier generation and transfer in the structure based on PBDTT-DPP:PC71BM:ITIC-F blend.

the LUMO level of PC71BM; it enables the stepwise hole transfer, but its contribution to the useful signal is negligible due to the low efficiency of hole generation and transfer in the acceptor material compared to the donor.

3. Conclusion

The technology was developed for fabrication of organic photosensitive structures of the visible and near infrared spectral ranges with a bulk heterojunction, and the influence of an additional acceptor in the structure was studied.

When studying the influence of the active layer composition based on the PBDTT-DPP:PC71BM blend, the samples with a donor-to-acceptor ratio of (1:2) exhibited the highest photosensitivity, demonstrating a spectral response in the wavelength range from 400 to 900 nm. However, the photosensitivity intensity was only 11 mA/W at $\lambda = 796$ nm, which is explained by the small difference between the LUMO levels of the donor and acceptor, limiting the built-in field. For the studied samples, the short-circuit current density was 0.16 mA/cm^2, and the open-circuit voltage was 0.5 V, the dark currents were 100 nA/cm^2.

To increase the intensity of the useful signal and extend the spectral range into the near-IR region, the fullerene derivative acceptor was replaced with the non-fullerene acceptor ITIC-F, which possesses a deeper LUMO level. The OPS based on PBDTT-DPP:ITIC-F blend demonstrated an extended sensitivity spectrum (450–1000 nm) with a maximum intensity of 100 mA/W (at $\lambda = 825$ nm). However, a dip is observed in the photosensitivity spectrum at a wavelength of 800 nm, which limits the potential application of the developed OPS. The short-circuit current density for the studied samples was 1.1 mA/cm^2, the open-circuit voltage was 0.75 V, and the dark current density was 130 nA/cm^2.

To eliminate the dip, a photosensitive structure based on the three-component blend PBDTT-DPP:PC71BM:ITIC-F was developed, combining the advantages of fullerene and non-fullerene acceptors. The introduction of PC71BM into the structure based on PBDTT-DPP:ITIC-F eliminated the dip at 800 nm and improved electron transport due to a stepwise transfer mechanism through both acceptors. As a result, the developed OPS demonstrated an operating spectral range of 400–950 nm, high photosensitivity of 130 mA/W at $\lambda = 818$ nm, and improved electrical characteristics: the short-circuit current density increased to 2.2 mA/cm^2 at an open-circuit voltage of 0.8 V, and the dark current decreased to 68 nA/cm^2. Analysis of charge carrier transfer pathways showed that the most efficient is the stepwise mechanism, where PC71BM acts as an intermediate step for electrons, simultaneously creating a barrier for holes and reducing their recombination probability.

Thus, this work demonstrates that the use of a three-component blend based on an organic donor and a combination of fullerene and non-fullerene acceptors allows simultaneously extending the spectral sensitivity range into the near-IR region and increasing the efficiency of charge carrier generation and collection by optimizing the morphology and energy levels of the materials comprising the active layer. The results of this work contribute to the development of

technologies for creating flexible and efficient photosensitive structures for the new generation.

Funding

The study was conducted as part of project No. FSEE-2025-0013.

Conflict of interest

The authors declare no conflict of interest.

References

[1] P.V. Pham, S.C. Lims, A. Kumar, R.K. Ulaganathan, R.I. Stantchev, R. Sankar. Chem. Eng. J., **522**, 167554 (2025). DOI: 10.1016/j.cej.2025.167554
[2] J. Chen, J. Wang, X. Li, J. Chen, F. Yu, J. He, J. Wang, Z. Zhao, G. Li, X. Chen, W. Lu. Sensors, **22** (2), 677 (2022). DOI: 10.3390/s22020677
[3] H. Ren, J.-D. Chen, Y.-Q. Li, J.-X. Tang. Adv. Sci., **8** (1), 2002418 (2021). DOI: 10.1002/advs.202002418
[4] Y. Wang, J. Kublitski, S. Xing, F. Dollinger, D. Spoltore, J. Benduhn, K. Leo. Mater. Horiz., **9**, 220 (2022). DOI: 10.1039/D1MH01215K
[5] M.C. Scharber, N.S. Sariciftci. Adv. Mater. Technol., **6** (4), 2000857 (2021). DOI: 10.1002/admt.202000857
[6] D. Neher, J. Kniepert, A. Elimelech, L.J.A. Koster. Sci. Rep., **6**, 24861 (2016). DOI: 10.1038/srep24861
[7] O.V. Mikhnenko, P.W.M. Blom, T.-Q. Nguyen. Energy Environ. Sci., **8**, 1867 (2015). DOI: 10.1039/C5EE00925A
[8] T. Shan, X. Hou, X. Yin, J.X. Guo. Front. Optoelectron., **15**, 49 (2022). DOI: 10.1007/s12200-022-00049-w
[9] M.D.M. Faure, B.H. Lessard. J. Mater. Chem. C, **9**, 14 (2021). DOI: 10.1039/D0TC04146G
[10] P.C.Y. Chow, T. Someya. Adv. Mater., **32** (15), 1902045 (2020). DOI: 10.1002/adma.201902045
[11] M.D. Pavlova, N.A. Khorshev, I.A. Lamkin, A.E. Degterev, I.A. Zorin, S.A. Tarasov. J. Opt. Technol., **92** (1), 48 (2025). DOI: 10.1364/JOT.92.000048
[12] G. Bhat, M. Kielar, P. Sah, A.K. Pandey, P. Sonar. Adv. Electron. Mater., **10** (2), 2300583 (2023). DOI: 10.1002/aelm.202300583
[13] M. Günther, N. Kazerouni, D. Blätte, J.D. Perea, B.C. Thompson, T. Ameri. Nat. Rev. Mater., **8**, 456 (2023). DOI: 10.1038/s41578-023-00545-1
[14] Q. Wang, Y. Zhang, Z. Wei. Chin. J. Chem., **41** (8), 958 (2023). DOI: 10.1002/cjoc.202200686
[15] S. Alam, J. Lee. Mater. Today Chem., **46**, 102718 (2025). DOI: 10.1016/j.mtchem.2025.102718
[16] S. Yuan, W. Luo, M. Xie, H. Peng. RSC Adv., **15** (4), 2470 (2025). DOI: 10.1039/D4RA08370A
[17] J. Jiang, H. Chen, H. Lin, C. Yu, S. Lan, C. Liu, K. Wei. Polym. Chem., **4**, 5321 (2013). DOI: 10.1039/C3PY00132F
[18] R. Ganesamoorthy, G. Sathiyan, P. Sakthivel. Sol. Energy Mater. Sol. Cells, **161**, 102 (2017). DOI: 10.1016/j.solmat.2016.11.024
[19] M. Casademont-Viñas, D. Capolat, A. Quesada-Ramírez, M. Reinfelds, G. Trimmel, M. Sanviti, J. Martín, A.R. Goñi, T. Kirchartz, M. Campoy-Quiles. J. Mater. Chem. A, **12**, 16716 (2024). DOI: 10.1039/D4TA01944J
[20] T. Li, G. Hu, L. Tao, J. Jiang, J. Xin, Y. Li, W. Ma, L. Shen, Y. Fang, Y. Lin. Sci. Adv., **9** (13), eadf6152 (2023). DOI: 10.1126/sciadv.adf6152
[21] M. Babics, H. Bristow, W. Zhang, A. Wadsworth, M. Neophytou, N. Gasparini, I. McCulloch. J. Mater. Chem. C, **9**, 2375 (2021). DOI: 10.1039/D0TC05341D
[22] L. Lv, J. Yu, X. Sui, J. Wu, X. Dong, G. Lu, X. Liu, A. Peng, H. Huang. J. Mater. Chem. C, **7** (19), 5739 (2019). DOI: 10.1039/C9TC00576E

Translated by M.Verenikina